HHS Public Access

Author manuscript

Biochemistry. Author manuscript; available in PMC 2017 April 12.

Published in final edited form as:

Biochemistry. 2016 April 12; 55(14): 2091–2099. doi:10.1021/acs.biochem.5b01109.

Effect of outer-sphere side chain substitutions on the fate of the *trans* iron-nitrosyl dimer in heme/nonheme engineered myoglobins (Fe_BMbs): Insights into the mechanism of denitrifying NO reductases

Hirotoshi Matsumura[†,§], **Saumen Chakraborty**[‡,§], **Julian Reed**[‖], **Yi Lu**[‡,‖], and **Pierre Moënne-Loccoz**[*,†]

[†]Division of Environmental and Biomolecular Systems, Institute of Environmental Health, Oregon Health and Science University

[‡]Department of Chemistry, University of Illinois at Urbana-Champaign

[‖]Department of Biochemistry, University of Illinois at Urbana-Champaign

Abstract

Denitrifying NO reductases are transmembrane protein complexes that utilize a heme/nonheme diiron center at their active sites to reduce two NO molecules to the innocuous gas N_2O. Fe_BMb proteins, with their nonheme iron sites engineered into the heme distal pocket of sperm whale myoglobin, are attractive models to study the molecular details of the NO reduction reaction. Spectroscopic and structural studies of Fe_BMb constructs have confirmed that they reproduce the metal coordination spheres observed at the active site of the cytochrome-*c*-dependent NO reductase from *Pseudomonas aeruginosa*. Exposure of Fe_BMb to excess NO, as examined by analytical and spectroscopic techniques, results primarily in the formation of a five-coordinate heme-nitrosyl complex without N_2O production. However, substitution of the outer-sphere residue Ile107 to a glutamic acid (i.e., I107E) decreases the formation rate of the five-coordinate heme-nitrosyl complex and allows for the sub-stoichiometric production of N_2O. Here, we aim to better characterize the formation of the five-coordinate heme-nitrosyl complex and to explain why the N_2O production increases with the I107E substitution. We follow the formation of the five-coordinate heme-nitrosyl inhibitory complex through the sequential exposure of Fe_BMb to different NO isotopomers using rapid-freeze-quench resonance Raman spectroscopy. The data show that the complex is formed by the displacement of the proximal histidine by a new NO molecule after the weakening of the Fe(II)-His bond in the intermediate six-coordinate low-spin heme-nitrosyl complex. These results lead us to explore diatomic migration within the scaffold of myoglobin and whether substitutions at residue 107 can be sufficient to control access to the proximal heme cavities. Results on a new Fe_BMb construct with an I107F substitution (Fe_BMb3) show an increased rate for the formation of the 5cLS heme-nitrosyl complex without N_2O

[*]Corresponding author: Pierre Moënne-Loccoz, Oregon Health & Science University, Institute of Environmental Health, 3181 SW Sam Jackson Park Road, Portland, Oregon 97239. Tel: 503-346-3429; Fax: 503-748-3427., moennelo@ohsu.edu.

[†]This work was supported by Grants GM74785 (P.M.-L.) and GM06221 (Y.L.) from the National Institutes of Health.

[§]Present address: Department of Life Science, Faculty and Graduate School of Engineering and Resource Science, Akita University, 1-1 Tegata Gakuen-machi, Akita City, Akita, 010-8502 Japan (T.H.) and Center for Integrated Nanotechnologies, Los Alamos National Lab, PO Box 1663, Albuquerque, NM 87545, United States (S.C.)

production. Taken together, our results suggest that production of N_2O from the [6cLS heme $\{FeNO\}^7/\{Fe_BNO\}^7$] *trans* iron-nitrosyl dimer intermediate requires a proton transfer event facilitated by out-sphere residue such as E107 in Fe_BMb2 and E280 in *Pseudomonas aeruginosa* cNOR.

The 2-electron reduction of nitric oxide (NO) to nitrous oxide (N_2O) by denitrifying ground bacteria is an essential step of the global nitrogen cycle and of great significance to global warming since agricultural production leads to atmospheric emission of the powerful greenhouse gas N_2O.(1) The biological reduction of NO is also of direct significance to human health since it allows pathogenic bacteria to fend off NO produced by the mammalian immune response.(2)

Two denitrifying NO reductases have been structurally characterized by X-ray crystallography, (3, 4) and in conjunction with many years of spectroscopic and kinetic analyses,(5-7) the basic outline of their catalytic cycle is now broadly accepted. Specifically, within the core of a transmembrane protein complex that is analogous to the heme/copper terminal oxidases of aerobic respiration,(8, 9) NO reductases anchor a heme/nonheme diiron(II) site that can react with two NO molecules to generate N_2O before the resulting diiron(III) center can be re-reduced by nearby electron-transfer cofactors. The two NOR crystal structures studied to date reveal a conserved hydrophobic channel leading to the diiron site that presumably permits rapid diffusion of NO and N_2O between the active site and the lipophilic bilayer of the biological membrane where the solubility of these gases is high. Accordingly, kinetic studies suggest that oxidation of the diiron(II) site by NO is a submillisecond process.(10)

Since nitroxyl (HNO), in contrast to NO, readily self-dimerizes to produce N_2O,(11) most proposed NOR mechanisms involve the initial binding of NO to iron(II) (i.e., at the heme or nonheme iron, or at both irons), where the NO is partially reduced to a nitroxyl prior to the formation of the N-N bond of a hyponitrite species;(12) however, neither the presence of this species nor its nitrosyl precursor(s) has been conclusively detected. The subsequent cleavage of an N-O bond to generate N_2O may proceed through protonation of the hyponitrite intermediate, or alternatively, isomerization of the coordinated hyponitrite to position an oxygen atom in a bridging coordination could lead to the formation of a bridging μ-oxo and the N_2O product. In the latter case, protonation of the μ-oxo bridge would occur along with the re-reduction of the diiron(III) site. Interestingly, while hydrophilic proton channels to the diiron sites have been modeled for both crystallized NORs, they are not conserved, and in fact provide access to different sides of the cytoplasmic membrane.(13)

Engineered myoglobins that mimic the heme/nonheme diiron site of NORs are attractive models to define the initial steps leading to N_2O production. High-resolution crystal structures of these constructs have confirmed that the coordination sphere of the two metals and the metal-metal distance observed in NORs are adequately reproduced.(14, 15) At the nonheme iron Fe_B site, two engineered distal histidines (L29H and F43H) and a glutamate side chain (V68E) complement the native distal histidine (H64) to provide the (3His, 1Glu) coordination sphere to the nonheme iron. While one myoglobin construct, Fe_BMb1, strictly provides the required side chains at the Fe_B site, a second construct, Fe_BMb2, also includes

a peripheral glutamate side chain that is believed to play a role in proton transfer during catalysis in NORs (Figure 1).

Using FTIR and resonance Raman (RR) spectroscopy, we have shown that Fe_BMb1 and Fe_BMb2 can bind one NO molecule with high-affinity at the heme iron(II) and that their resulting six-coordinate low-spin (6cLS) heme-nitrosyl complexes (heme $\{FeNO\}^7$ species in the notation of Enemark and Feltham),(16) exhibit exceptionally low N-O stretching frequencies between 1545 and 1550 cm^{-1}, which we attribute to a strong nitroxyl-like character.(17) In addition, we found that equally low N-O stretching frequencies are observed when their Fe_B sites are occupied with either Fe(II) or Zn(II), but not with Cu(I), suggesting that the 6cLS heme nitroxyl-like complexes are stabilized by electrostatic interactions with the divalent metal center at their Fe_B sites. (17)

This semi-bridging nitroxyl-like structure was predicted by theoretical calculations and is expected to increase the nucleophilicity of the NO^- group to promote a direct electrophilic attack by a second NO to produce a diferric-hyponitrite dianion intermediate.(12, 18) However, monitoring the reactions of Fe_BMb constructs with excess NO using UV-vis stopped-flow absorption and rapid-freeze-quench resonance Raman (RFQ-RR) spectroscopies (between 10 and 90-fold excess NO in stopped-flow experiments and 3- to 4-fold NO excess in RFQ) and showed that a direct attack of the nitroxyl-like species by NO does not occur.(19) Specifically, time-resolved measurements show that the heme and non-heme iron(II) each binds one NO molecule to form a [6cLS heme $\{FeNO\}^7/\{Fe_BNO\}^7$] *trans* iron-nitrosyl dimer complex and that this complex accumulates in the millisecond time scale whether the Fe_BMb constructs are directly exposed to excess NO in their diiron(II) forms or if the heme-nitrosyl complex is pre-formed by the addition of 1-equiv NO (Scheme 1). The formation rates for these *trans* iron-nitrosyl dimers are complex. The first event corresponds to the binding of one NO to Fe_B(II) within the millisecond time resolution of our stopped-flow and RFQ instruments.(19) In wild-type myoglobin, access to the heme in the distal pocket is gated by the distal histidine His64,(20) but in the Fe_BMb constructs, His64 is recruited as an Fe_B(II) ligand, and preferential binding of the first NO to Fe_B(II) rather than to the heme iron(II) may simply reflect a favorable orientation of the open coordination site on Fe_B(II) relative to the entry of NO into the distal pocket. In the absence of excess NO, the NO group migrates from Fe_B(II) to the heme iron(II), indicating a higher NO binding constant for the heme iron(II) relative to Fe_B(II) (Scheme 1). Accordingly, the dissociation rate constants for NO in these heme-nitrosyl complexes are low: 0.1×10^{-3} and 0.5×10^{-5} s^{-1} in Fe_BMb1 and Fe_BMb2, respectively.(19) After binding of a first NO molecule at Fe_B, a second NO molecule binds to the heme iron(II) with a biphasic rate, possibly reflecting alternative access routes or alternative geometries at the distal pocket. The resulting *trans* iron-nitrosyl dimer complexes exhibit a single set of heme and nonheme N-O stretching frequencies in both Fe_BMb constructs.(19)

Quantitative detection of N_2O in solution by transmittance FTIR spectroscopy indicated that the *trans* iron-nitrosyl dimer in Fe_BMb1 does not produce N_2O but instead decays with the formation of a five-coordinate low-spin (5cLS) complex in an NO-concentration dependent fashion.(19) The same 5cLS heme-nitrosyl complex forms in Fe_BMb2 as well, but it does so at a slower rate and in a sub-stoichiometric fashion since in contrast to Fe_BMb1,

approximately half an equivalent of N_2O is produced with a first order rate constant of 0.7 s^{-1} at 4 °C (Scheme 1). Although only 0.5 equivalent of N_2O is produced in Fe_BMb2, it nevertheless validates the potential of these models to mimic denitrifying NORs. To further engineer these myoglobin constructs toward efficient NO reduction, we must first understand the mechanistic pathway for the formation of the 5cLS heme-nitrosyl complex and the molecular basis for the increased reactivity of the *trans* iron-nitrosyl dimer toward N-N bond formation in Fe_BMb2.

Here, we show RFQ-RR data that support a proximal attack of the heme iron-histidine bond by NO as the mechanistic route to the 5cLS heme-nitrosyl complex. Because prior studies of diatomic ligand migration within myoglobin have shown that the heme proximal site is accessed primarily through the distal pocket rather than directly from solvent and that residue 107 can control ligand migration,(21-23) we also explore a new construct where isoleucine 107 is substituted with a phenylalanine (Fe_BMb3). The I107F substitution in swMb was shown to limit diffusion of CO from the heme distal pocket to the proximal side.(24) However, with the Fe_BMb framework, we find that the added Phe sidechain does not preclude the inhibitory NO attack of the proximal pocket and that in fact it accelerates the formation rate of the 5cLS heme-nitrosyl complex. The current study supports the notion that the added hydrophilicity the I107E mutation provides to the distal pocket is at the origin of the gain in NO reductase activity in Fe_BMb2 and further supports the importance of proton transfer to the formation of the N-N bond in NORs.

Materials and Methods

Fe_BMbs preparation and Fe(II) loading

Fe_BMb3 (swMb L29H/F43H/V68E/I107F) was constructed using the procedure described previously,(14, 15) and confirmed by DNA sequencing at the Biotechnology Center of the University of Illinois. Fe_BMb1 (swMb L29H/F43H/V68E) and Fe_BMb3 constructs were expressed and purified in the oxidized form (i.e. metMb) with empty Fe_B sites as described previously. The purity and identity were confirmed by SDS-PAGE and protein concentrations were calculated on the basis of a 406-nm extinction coefficient, ε_{406}, of 175 $mM^{-1}cm^{-1}$ in the oxidized form. 1 mM apo-Fe_BMbs solutions in 50 mM Bis-Tris buffer, pH 7, were brought into an anaerobic glovebox containing <1 ppm of O_2 (Omnilab System, Vacuum Atmospheres Co.). The proteins were reduced by addition of ~5 mM sodium dithionite followed by removal of excess reduction agents with desalting spin columns (7K MWCO, Zeba, Thermo Scientific). The Fe(II) loading into apo-Fe_BMbs was performed according to the previously described methods. Briefly, 1.3 equivalent $Fe(II)Cl_2$ in 0.01 M HCl was added to 1 mM reduced apo-Fe_BMbs solutions at a rate of 0.5 μL/min with gentle stirring and the protein solution was anaerobically incubated at room temperature for 20 min. After the incubation, the excess iron was removed with a 7K MWCO desalting spin column. Iron incorporation into the Fe_B site of Fe_BMbs was confirmed by UV-vis spectroscopy using a Cary 50 spectrophotometer (Varian Inc).

Preparation of NO solution and preparation of NO adducts

NO gas (99.5%, Airgas) and ^{15}NO gas (>98% ^{15}N, Cambridge Isotope Laboratory) were further purified by bubbling through a 1 M NaOH solution to remove the degradation products N_2O_3 and NO_2. The NO-saturated solutions (~2 mM) were prepared by bubbling the purified NO gases through 50 mM Bis-Tris buffer with septa inside the anaerobic glovebox. The exact concentration of NO solutions was determined by titration against deoxymyoglobin in UV-vis cuvettes with septa. To prepare Fe_BMb samples fully reacted with NO, the sample headspace was thoroughly exchanged with the purified NO gases, and the completeness of the reaction was checked by UV-vis spectra collected directly in UV-vis cuvettes or NMR tubes.

RR Experiments

RR spectra were recorded using a custom McPherson 2061/207 spectrograph (set at 1 m focal length with 2400 grooves per millimeter of holographic gratings) equipped with a liquid N_2-cooled CCD detector (LN-1100PB, Princeton Instruments). The 406-nm excitation laser was derived from a Kr laser (Innova 302C, Coherent). A Kaiser Optical supernotch filter or a long-pass filter (RazorEdge, Semrock) was used to attenuate Rayleigh scattering. Low temperature spectra were recorded in a backscattering geometry on samples maintained at 110 K with a coldfinger dipped in a liquid nitrogen Dewar. Frequencies were calibrated relative to aspirin and are accurate to ±1 cm^{-1}. To assess the photosensitivity of the NO adducts, rapid acquisitions within a range of laser powers and continuous sample spinning were compared with longer data acquisitions on static samples. Because none of the RFQ samples showed evidence of photosensitivity under laser illumination at 110 K, RR spectra could be obtained on static samples with laser power as high as 100 mW defocused on a 0.5 mm width by 1 mm height sample area. Each RR spectra correspond to CCD total exposure times of 5 min. Background subtractions were strictly limited to 2-point linear baselines applied to the entire 1100-pixel window.

Rapid-Freeze-Quench (RFQ) Experiments

RFQ experiments were conducted according to our previously described protocol with some modifications.(25) ^{14}NO-mononitrosyl complex of Fe_BMb1 was prepared by stoichiometric addition of ^{14}NO to fully reduced protein using ^{14}NO-saturated stock solution and checked by UV-vis spectra just prior to the sample loading. Glass syringes (1 mL) were loaded with protein solutions (0.6 mM ^{14}NO-mononitrosyl complex of FeMb1 in 50 mM Bis-Tris, pH 7.0) and 2 mM NO solution (50 mM Bis-Tris, pH 7.0) inside the anaerobic glovebox. The sample syringes were mounted to a System 1000 Chemical/Freeze Quench Apparatus (Update Instruments) and equilibrated at 4 °C. Reaction times were controlled by varying the syringe displacement rate from 1 to 8 cm/s or by varying the length of the reactor hose between the mixer and the exit nozzle. Five milliseconds were added to the calculated reaction times to account for the time-of-flight and the freezing time in liquid ethane. Mixed volumes of 300 μL were ejected into a glass funnel attached to NMR tubes filled with liquid ethane, and the frozen samples were packed into the tube as the assembly sat within a Teflon block cooled to −120 °C. The cryosolvent was allowed to evaporate from packed samples by incubation at −80 °C for 2 h before RR measurements.

Stopped-Flow UV-vis Spectroscopy

Stopped-flow experiments were performed with an SX20 apparatus (Applied Photophysics) with a 1-cm path length cell equilibrated at 4 °C inside an anaerobic glovebox. Fe_BMb stock solutions were diluted to obtain a final concentration of 10 μM in 50 mM Bis-Tris buffer, pH 7.0. NO solutions ranging from 0.1 to 2 mM in the same buffer were prepared in 1.2 mL glass vials capped with septa and were used immediately. After each experiment, remaining premixed solutions were recovered from the stopped-flow apparatus to confirm the concentration of the reactants. The single-wavelength data at 388, 420, and 440 nm were fit using Pro-Data software from Applied Photophysics or Origin 9.0 software by Origin Lab Corporation. Initial estimates of rate constants and amplitudes were derived from either single- or multiple- exponential fits to these single wavelength data sets. The kinetics data were better fit to triple exponential leading to pseudo-first-order rate constants k_{obs1}, k_{obs2}, and k_{obs3}. The reported rate constants are from global analyses and are the average of at least three different rapid mixing experiments. Second-order rate constants were obtained from linear regression analyses of k_{obs} versus NO concentration plots.

Results and Discussion

RFQ-RR evidence for the formation of the 5cLS heme-nitrosyl complex through a proximal attack of the heme 6cLS heme-nitrosyl by NO

Our previous stopped-flow and RFQ-RR study of the reaction of reduced Fe_BMb1 with a 3- to 4-fold NO excess demonstrated that a [6cLS heme $\{FeNO\}^7/\{Fe_BNO\}^7$] *trans* iron-nitrosyl dimer complex forms within the millisecond scale before it decays to a [5cLS heme $\{FeNO\}^7/\{Fe_BNO\}^7$] complex.(19) Stopped-flow absorption data revealed that the conversion of the heme-nitrosyl complex from a six- to five-coordinate number is linearly dependent on NO concentrations with a 2.1 $mM^{-1}s^{-1}$ second order rate constant that implies the involvement of a third NO molecule.(19) However, it is unknown if this third NO acts in an allosteric fashion to destabilize the 6cLS heme-NO complex and promote the iron-histidine bond cleavage (Scheme 1, allosteric effect), or if NO directly attacks the heme proximal pocket to displace the proximal histidine (Scheme 1, proximal attack). Unfortunately, the RR signature of the 5cLS heme-nitrosyl does not provide any direct insight as to whether the nitrosyl group is bound on the distal or proximal side.

To define the route of formation of the 5cLS heme-nitrosyl complex in Fe_BMb1, we prepared RFQ samples with different freezing times in the course of the reaction of $Fe_BMb1(^{14}NO)$ with excess ^{15}NO for analysis by low-temperature RR spectroscopy. We previously reported that exposure of reduced Fe_BMb1 to 1 equiv NO produces a 6cLS heme-nitrosyl adduct with a half-life of 2 h at room temperature which gives ample time to prepare the mononitrosyl complex and test its reaction with isotopically labeled ^{15}NO excess by RFQ-RR.(17, 19) The slow NO dissociation rate of the 6cLS heme-nitrosyl complex in $Fe_BMb1(NO)$ also precludes exchange of the distal NO with free NO within the millisecond to second timescale explored by RFQ. Indeed, the exchange of NO from the 6cLS heme $\{FeNO\}^7$ complex of horse heart myoglobin with free NO was shown to depend on a dissociative mechanism and to proceed very slowly with a half-life of ~2 h at 40 °C.(26, 27) Thus, if the end-product results from an allosteric effect of NO, the ^{14}NO from the 6cLS

heme-nitrosyl complex should be retained in the 5cLS heme-nitrosyl complex, but if the dissociation of the proximal histidine occurs through a displacement mechanism by a third NO molecule, a 5cLS heme-^{15}NO complex is expected.

Figure 2 compares the RR spectra of three RFQ samples trapped 40 ms, 280 ms, and 2 min after mixing $Fe_BMb1(^{14}NO)$ with excess ^{15}NO. The spectrum of the 40-ms RFQ sample exhibits prominent porphyrin skeletal modes ν_4, ν_3, ν_2, and ν_{10} at 1376, 1506, 1586, and 1644 cm^{-1}, respectively, characteristic of a 6cLS heme-nitrosyl species,(28) with only a minor ν_4 at 1354 cm^{-1} corresponding to a small population of unreacted ferrous 5cHS porphyrin (Figure 2, middle panel). In the low-frequency region, the RR spectrum of the 40-ms RFQ sample shows a 572-cm^{-1} band previous assigned to the $\nu(Fe^{14}NO)$ from the 6cLS heme $\{FeNO\}^7$ complex based on its 20-cm^{-1} downshift with ^{15}NO (Figure 2, left panel).(19) In the high-frequency region, beyond the porphyrin skeletal modes, a very weak signal at 1726 cm^{-1} assigned in our previous work(19) to a $\nu(^{15}NO)$ from a nonheme $\{Fe_B{}^{15}NO\}^7$ species is also observed with unchanged intensity for all three spectra of different RFQ samples (Figure 2, right panel). Thus, these RR spectra are consistent with the rapid binding of ^{15}NO to the nonheme iron to formation a *trans* [6cLS heme $\{Fe^{14}NO\}^7/\{Fe_B{}^{15}NO\}^7$] complex.

The RR spectrum of the 280-ms RFQ sample shows porphyrin ν_3 and ν_{10} modes at 1506 and 1644 cm^{-1} that gains further intensity in the RR spectrum of the 2-min RFQ sample and reflect the conversion of the 6cLS heme-nitrosyl to a 5cLS heme-nitrosyl species.(19) Most importantly, in the low-frequency region, the 572 cm^{-1} band from the initial 6cLS heme $\{FeNO\}^7$ species is replaced by a 511 cm^{-1} band previously assigned to the $\nu(Fe^{15}NO)$ from the 5cLS heme-nitrosyl complex (Table 1).(19) Thus, the RFQ-RR data demonstrate that after binding of a first ^{15}NO molecule to the nonheme Fe_B site to form the *trans* iron-nitrosyl dimer complex, i.e., [6cLS heme $\{Fe^{14}NO\}^7/\{Fe_B{}^{15}NO\}^7$], a second ^{15}NO molecule binds at the proximal heme iron site, displacing the histidine ligand before release of the distal ^{14}NO molecules (Scheme 1, proximal attack pathway).

Characterization of Fe_BMb3, an I107 variant that fails to produce N_2O

RFQ-RR spectroscopy of the reaction of ^{14}NO-mononitrosyl Fe_BMb1 with ^{15}NO strongly suggests a proximal NO as the driving force for the 6cLS to 5cLS conversion of the heme-nitrosyl complex. As previously reported,(14, 19) substituting the outer sphere residue Ile107 to a glutamate affects the fate of the NO reaction at the heme/nonheme diiron site. Specifically, the binding sequence for the first two NO molecules generating the *trans* [6cLS heme $\{FeNO\}^7/\{Fe_BNO\}^7$] iron-nitrosyl dimer complex remains unchanged in this Fe_BMb2 construct compared to Fe_BMb1, but conversion of this intermediate to the 5cLS heme-nitrosyl complex is not complete and instead half the iron-nitrosyl dimer decays with production of N_2O.(14, 19) There is no significant change in van der Waals volume for an Ile-to-Glu substitution, but perturbations in electrostatic and hydrogen bond interactions are expected, and interestingly, the crystal structure of Fe_BMb2 indicates that the added glutamate side chain stabilizes a coordinating water molecule at the Fe_B site. Thus, a possible explanation for the impact of the I107E substitution on the fate of the reaction is that it facilitates protonation steps required for NO reduction.(14)

An alternative explanation is that the I107E substitution limits the migration of diatomic ligands from the distal to proximal side of the heme pocket and protects the heme Fe-His bond from NO. Indeed, the second order rate constant for the formation of the 5cLS heme-nitrosyl complex in Fe_BMb2 is 2-times lower than in Fe_BMb1, and this change may suffice to allow the productive reaction to proceed. Spectroscopic and crystallographic studies of wild-type swMb have shown that Ile107 lines the heme cavity and controls the migration of diatomic ligands from the distal pocket to proximal cavities that are otherwise mostly inaccessible from outside the protein matrix.(24, 29, 30) Specifically, an I107F mutation was shown to limit migration of CO from the distal side to the proximal cavities.(24) Thus, we tested a new Fe_BMb construct with an I107F substitution (Fe_BMb3) by stopped-flow and RR spectroscopy.

As with Fe_BMb1 and Fe_BMb2, incorporation of Fe(II) at the Fe_B site of Fe_BMb3 can be monitored by UV-vis spectroscopy at it induced the appearance of prominent shoulders at 524 and 578 nm in the α/β bands region of the visible spectrum (Figure 3). Exposure of reduced Fe_BMb3 to excess NO results in a major blue shift of the Soret absorption to 406 nm, suggesting formation of a 5cLS heme nitrosyl species as in Fe_BMb1 (Figure 3). This product was further characterized by low-temperature RR spectroscopy. The high frequency RR spectra show ν_4, ν_3, ν_2, and ν_{10} modes at 1377, 1507, 1587, and 1610 cm^{-1}, respectively, characteristic of a 5cLS heme-nitrosyl species (Figure 4). RR bands at 1658 and 524 cm^{-1} that shift to 1626 and 512 cm^{-1} with ^{15}NO are assigned to the ν(NO) and ν(FeNO) modes, respectively. These vibrational frequencies are typical of a 5cLS heme $\{FeNO\}^7$ species and within a few wavenumbers from those observed in Fe_BMb1.(19) Beyond the range of porphyrin skeletal modes, a very weak bands at 1752 cm^{-1} that shifts to 1720 cm^{-1} with ^{15}NO is assigned to the ν(NO) from $\{Fe_BNO\}^7$, within 3-cm^{-1} of the 1755 cm^{-1} frequency previously measured in Fe_BMb1.(19) Thus, Fe_BMb3 forms equivalent [5cLS heme $\{FeNO\}^7$/$\{Fe_BNO\}^7$] nitrosyl dimer complexes as Fe_BMb1 and Fe_BMb2 when exposed to 3 or more NO equivalents.

RR spectra of RFQ samples for the reaction of Fe_BMb3 with a 3-fold NO excess indicates that, as with other Fe_BMbs, a first NO molecule binds to the nonheme iron with a ν(NO) at 1753 cm^{-1}, before binding of a second NO to the 5cHS ferrous heme which shift the porphyrin ν_4 mode from 1354 to 1377 cm^{-1} (Figure 5). In the low-frequency region, the ν(FeNO) mode from the transient 6cLS heme-nitrosyl complex is only weakly enhanced but detectable through its $^{14}NO/^{15}NO$ isotope dependence at 563 cm^{-1} before its conversion to the 5cLS heme $\{FeNO\}^7$ end-product (Figure 5). The reaction of reduced Fe_BMb3 with NO was also monitored by stopped-flow absorption at 4 °C, with a fixed protein concentration of 5 μM and varying NO concentrations of ~50 μM to 1 mM under pseudo-first-order conditions. Initial kinetic phases show a blue-shift of the ferrous HS heme Soret absorption from 434 nm to 425 nm followed by a further blue shift to 408 nm on a second time scale (Figure 6). As previously observed with Fe_BMb1 and Fe_BMb2,(19) the initial Soret blue shift is multiphasic with single wavelength analyses leading to observed rates with linear dependence on NO concentration and second-order rate constants k_1 ~463 mM^{-1} s^{-1} and k_2 = 11 mM^{-1} s^{-1}. The last kinetic phase corresponds to a further blue shift of the Soret absorption from 425 to 408 nm and is monophasic with a second-order rate k_3 = 5.3 mM^{-1} s^{-1}. Thus, this last step which corresponds to the conversion of the 6cLS heme-nitrosyl

complex to a 5cLS heme-nitrosyl occurs more than twice as fast with the I107F substitution (i.e., k_3 = 2.1 mM^{-1} s^{-1} in Fe_BMb1).

In view of the increased rate of conversion of the heme-nitrosyl complex from six- to five-coordinate in Fe_BMb3, we collected low-frequency RR spectra of reduced Fe_BMb3 with a 442 nm excitation to measure the ν(Fe-N_{His}) mode. The spectrum reveals a relatively minor 2-cm^{-1} downshift of the ν(Fe-N_{His}) mode in Fe_BMb3 relative to Fe_BMb1 and Fe_BMb2 (Figure 7).(17) A more substantial shift is observed in the 450-cm^{-1} region where porphyrin vinyl C-C-C bending modes are detected. Specifically, a mode observed at 435 cm^{-1} in wild-type smMb and that is unchanged in Fe_BMb1 is detected at 420 cm^{-1} in Fe_BMb3. Correlating this 15-cm^{-1} downshift to a precise structural perturbation is not straightforward since RR analyses of heme isotopomers in swMb have assigned this mode to the C_2-vinyl bending mode with some coupling with the bending of the nearby C_1-methyl.(31) Nevertheless, the spectral downshifts of the $\delta(C_\beta C_a C_b)_2$ mode in Fe_BMb3 and Fe_BMb2 (−15 and −4 cm^{-1}, respectively) are consistent with the close vicinity of residue 107 with the porphyrin's pyrrole ring A.

Overall, these RR data indicate that the increased rate of six- to five-coordinate heme-nitrosyl conversion in Fe_BMb3 is not due to a weakening of the iron-histidine bond but rather to a configuration of the Phe side chain that facilitates migration of NO from the distal to proximal pocket. Thus, the previously reported effect of the I107F substitution on diatomic migration within the Mb framework is not observed here, which a posteriori is not too surprising when one consider the extent of distal pocket rearrangement resulting from the engineering of the Fe_B site.

Conclusion

Using RFQ-RR spectroscopy, we have defined the route of formation of the 5cLS heme-nitrosyl complex in Fe_BMb constructs. Specifically, the RFQ-RR analysis shows that the distal NO group of the 6cLS heme-nitrosyl precursor is not retained in the 5cLS heme-nitrosyl complex. Because NO ligand exchange at the heme distal coordination site is expected to be kinetically inert,(27) the RFQ-RR data imply that the 5cLS heme-nitrosyl complex is formed through a proximal attack of the iron-histidine bond by a new NO molecule. Such displacement of proximal histidine by a second NO molecule through a bis-nitrosyl transition state have been proposed previously in soluble guanylate cyclase and in cytochrome c'.(32-35) While evidence for the formation of transient bis-nitrosyl heme complexes are lacking in heme proteins, evidence for the formation of such complexes in synthetic heme systems have been reported.(36)

Clearly, a proximal 5cLS heme-nitrosyl complex will not react with the nonheme $\{Fe_BNO\}^7$ complex on the opposite side of the heme plane to produce N_2O. This lack of reactivity is consistent with the high stability of the [5cLS heme $\{FeNO\}^7$/$\{Fe_BNO\}^7$] complex which we characterized by RR at both ambient and cryogenic temperatures in Fe_BMb1(14, 19) and Fe_BMb3 (Figure 6). Preventing NO access to the proximal pocket could improve the production of N_2O from these Fe_BMb systems. However, filling the proximal cavity through point mutations is not a simple option since, apart from the heme and proximal histidine, the

cavity is lined by one isoleucine and two leucine residues rather than small hydrophobic residues.(29, 30) Increasing the dielectric constant of the proximal cavity by substitution of one Leu/Ile with a hydrophilic residue may allow solvent molecules to fill the cavity, but it would also decrease the hydrophobicity of the heme pocket and weaken the heme binding affinity of the construct. Mutation at the I107 residues are known to affect the migrations of diatomic ligands from the heme distal pocket to the heme proximal cavity, and accordingly the rate of formation of the 5cLS heme-nitrosyl complex in Fe_BMb2 and Fe_BMb3 differs significantly from that of Fe_BMb1, but they do not fully suppress the proximal histidine displacement.

Cleavage of the covalent bond between the heme iron and the proximal histidine also occur at the diiron active site of denitrifying NO reductases. In the resting state of oxidized *Paracoccus dentrificans* cNOR, the catalytic heme is a five-coordinate high-spin heme iron(III) bridged to Fe_B(III) by a μ-oxo ligand.(37, 38) RFQ-EPR monitoring of the reaction of NO with *Pseudomonas aeruginosa* cNOR revealed a signal at $g \sim 2$ with ^{14}N-hypefine splitting parameter suggestive of a 5cLS heme-nitrosyl species that decayed within 10 ms. (10) Moreover, the reduced Fe_BMb constructs exhibit heme ν(Fe-N_{His}) stretching modes between 211 and 213 cm^{-1} which closely match the 218 cm^{-1} frequency observed in *Paracoccus denitrificans* cNOR.(37) Thus, nothing suggests that the heme proximal histidine in the Fe_BMb constructs might be excessively labile relative to that of the catalytic heme in cNORs. Instead, and despite the close structural similarity of the diiron sites of the Fe_BMb constructs and cNORs, it is evident that Fe_BMb2 produces N_2O too slowly to prevent free NO to access the heme distal pocket and prevent the completion of the NO reduction reaction. Indeed, while steady-state turnover numbers for cNORs can reach 40 s^{-1},(39-41) Fe_BMb2 produces N_2O only at a rate of 0.7 s^{-1} at 4 °C.

Blomberg and Siegbahn have used computational calculations to modeled the generation of N_2O at the heme/nonheme diiron site of cNOR and concluded that the diferrous center could reduce two NO molecules without requirement for additional proton or electron;(12) in this mechanistic model, the conserved peripheral glutamate, mimicked by I107E in Fe_BMb2, is only involved in proton transfer to the diferric μ-oxo bridged cluster as it is re-reduced though internal electron transfer by the low-spin heme *b* and *c*.(12) However, the total lack of NO reduction in Fe_BMb1 and in Fe_BMb3 with the I107F substitution suggests that the production of N_2O in Fe_BMb2 with the I107E substitution might benefit from the increased hydrophilicity at the distal pocket. Since all three constructs transit through the [6cLS heme $\{FeNO\}^7/\{Fe_BNO\}^7$] *trans* iron-nitrosyl dimer complex, it is tempting to suggest that protonating $\{FeNO\}^8$ and/or iron-hyponitrite species is essential to the formation of the N-N bond and cleavage of the N-O bond required to produce N_2O.

Abbreviations

NOR	nitric oxide reductase
swMb	sperm whale myoglobin
Fe_BMb1	swMb L29H/F43H/V68E variant

Fe_BMb2	swMb L29H/F43H/V68E/I107E variant
Fe_BMb3	swMb L29H/F43H/V68E/I107F variant
RR	resonance Raman
RFQ	rapid-freeze-quench
FTIR	Fourier transform infra-red

REFERENCES

1. Galloway JN, Dentener FJ, Capone DG, Boyer EW, Howarth RW, Seitzinger SP, Asner GP, Cleveland CC, Green PA, Holland EA, Karl DM, Michaels AF, Porter JH, Townsend AR, Vöosmarty CJ. Nitrogen Cycles: Past, Present, and Future. Biogeochemistry. 2004; 70:153–226.
2. Stevanin TM, Laver JR, Poole RK, Moir JW, Read RC. Metabolism of nitric oxide by *Neisseria meningitidis* modifies release of NO-regulated cytokines and chemokines by human macrophages. Microbes. Infect. 2007; 9:981–987. [PubMed: 17544805]
3. Hino T, Matsumoto Y, Nagano S, Sugimoto H, Fukumori Y, Murata T, Iwata S, Shiro Y. Structural basis of biological N2O generation by bacterial nitric oxide reductase. Science. 2010; 330:1666–1670. [PubMed: 21109633]
4. Matsumoto Y, Tosha T, Pisliakov AV, Hino T, Sugimoto H, Nagano S, Sugita Y, Shiro Y. Crystal structure of quinol-dependent nitric oxide reductase from Geobacillus stearothermophilus. Nat. Struct. Mol. Biol. 2012; 19:238–245. [PubMed: 22266822]
5. Wasser IM, de Vries S, Moënne-Loccoz P, Schroder I, Karlin KD. Nitric oxide in biological denitrification: Fe/Cu metalloenzyme and metal complex NO_x redox chemistry. Chem. Rev. 2002; 102:1201–1234. [PubMed: 11942794]
6. Moënne-Loccoz P. Spectroscopic characterization of heme iron-nitrosyl species and their role in NO reductase mechanisms in diiron proteins. Natl. Prod. Rep. 2007; 24:610–620.
7. Watmough NJ, Field SJ, Hughes RJ, Richardson DJ. The bacterial respiratory nitric oxide reductase. Biochem. Soc. Trans. 2009; 37:392–399. [PubMed: 19290869]
8. van der Oost J, de Boer AP, de Gier JW, Zumft WG, Stouthamer AH, van Spanning RJ. The heme-copper oxidase family consists of three distinct types of terminal oxidases and is related to nitric oxide reductase. FEMS Microbiol. Lett. 1994; 121:1–9. [PubMed: 8082820]
9. de Vries S, Schroder I. Comparison between the nitric oxide reductase family and its aerobic relatives, the cytochrome oxidases. Biochem. Soc. Trans. 2002; 30:662–667. [PubMed: 12196159]
10. Kumita H, Matsuura K, Hino T, Takahashi S, Hori H, Fukumori Y, Morishima I, Shiro Y. NO reduction by nitric oxide reductase from denitrifying bacterium *Pseudomonas aeruginosa*: characterization of reaction intermediates that appear in the single turnover cycle. J. Biol. Chem. 2004; 279:55247–55254. [PubMed: 15504726]
11. Shafirovich V, Lymar SV. Nitroxyl and its anion in aqueous solutions: spin states, protic equilibria, and reactivities toward oxygen and nitric oxide. Proc Natl Acad Sci U S A. 2002; 99:7340–7345. [PubMed: 12032284]
12. Blomberg MR, Siegbahn PE. Mechanism for N_2O generation in bacterial nitric oxide reductase: a quantum chemical study. Biochemistry. 2012; 51:5173–5186. [PubMed: 22680334]
13. Tosha T, Shiro Y. Crystal structures of nitric oxide reductases provide key insights into functional conversion of respiratory enzymes. IUBMB life. 2013; 65:217–226. [PubMed: 23378174]
14. Lin YW, Yeung N, Gao YG, Miner KD, Tian S, Robinson H, Lu Y. Roles of glutamates and metal ions in a rationally designed nitric oxide reductase based on myoglobin. Proc. Natl. Acad. Sci. U. S. A. 2010; 107:8581–85816. [PubMed: 20421510]
15. Yeung N, Lin YW, Gao YG, Zhao X, Russell BS, Lei L, Miner KD, Robinson H, Lu Y. Rational design of a structural and functional nitric oxide reductase. Nature. 2009; 462:1079–1082. [PubMed: 19940850]

16. Enemark JH, Feltham RD. Principles of structure, bonding, and reactivity for metal nitrosyl complexes. Coord. Chem. Rev. 1974; 13:339–406.
17. Hayashi T, Miner KD, Yeung N, Lin YW, Lu Y, Moënne-Loccoz P. Spectroscopic characterization of mononitrosyl complexes in heme--nonheme diiron centers within the myoglobin scaffold (Fe(B)Mbs): relevance to denitrifying NO reductase. Biochemistry. 2011; 50:5939–5947. [PubMed: 21634416]
18. Blomberg LM, Blomberg MR, Siegbahn PE. Reduction of nitric oxide in bacterial nitric oxide reductase-a theoretical model study. Biochim. Biophys. Acta. 2006; 1757:240–252. [PubMed: 16774734]
19. Matsumura H, Hayashi T, Chakraborty S, Lu Y, Moënne-Loccoz P. The production of nitrous oxide by the heme/nonheme diiron center of engineered myoglobins (Fe(B)Mbs) proceeds through a trans-iron-nitrosyl dimer. J Am Chem Soc. 2014; 136:2420–2431. [PubMed: 24432820]
20. Rohlfs RJ, Mathews AJ, Carver TE, Olson JS, Springer BA, Egeberg KD, Sligar SG. The effects of amino acid substitution at position E7 (residue 64) on the kinetics of ligand binding to sperm whale myoglobin. J Biol Chem. 1990; 265:3168–3176. [PubMed: 2303446]
21. Frauenfelder H, McMahon BH, Austin RH, Chu K, Groves JT. The role of structure, energy landscape, dynamics, and allostery in the enzymatic function of myoglobin. Proc Natl Acad Sci U S A. 2001; 98:2370–2374. [PubMed: 11226246]
22. Frauenfelder H, McMahon BH, Fenimore PW. Myoglobin: the hydrogen atom of biology and a paradigm of complexity. Proc Natl Acad Sci U S A. 2003; 100:8615–8617. [PubMed: 12861080]
23. Yu TQ, Lapelosa M, Vanden-Eijnden E, Abrams CF. Full kinetics of CO entry, internal diffusion, and exit in myoglobin from transition-path theory simulations. J Am Chem Soc. 2015; 137:3041–3050. [PubMed: 25664858]
24. Lamb DC, Nienhaus K, Arcovito A, Draghi F, Miele AE, Brunori M, Nienhaus GU. Structural dynamics of myoglobin: ligand migration among protein cavities studied by Fourier transform infrared/temperature derivative spectroscopy. J Biol Chem. 2002; 277:11636–11644. [PubMed: 11792698]
25. Matsumura H, Moenne-Loccoz P. Characterizing millisecond intermediates in hemoproteins using rapid-freeze-quench resonance Raman spectroscopy. Methods in molecular biology. 2014; 1122:107–123. [PubMed: 24639256]
26. Andersen HJ, Johansen HS, Shek CK, Skibsted LH. Nitric oxide exchange in nitrosylmyoglobin. Z. Lebensm.-Unters. Forsch. 1990; 191:293–298. [PubMed: 2293519]
27. Moller JKS, Skibsted LH. Nitric Oxide and Myoglobins. Chem. Rev. (Washington, D. C.). 2002; 102:1167–1178.
28. Spiro, TG. Resonance Raman Spectroscopy of Metalloporphyrins. Vol. Vol. 3. John Wiley & Sons; New York: 1988.
29. Schlichting I, Berendzen J, Phillips GN Jr. Sweet RM. Crystal structure of photolysed carbonmonoxy-myoglobin. Nature. 1994; 371:808–812. [PubMed: 7935843]
30. Ostermann A, Waschipky R, Parak FG, Nienhaus GU. Ligand binding and conformational motions in myoglobin. Nature. 2000; 404:205–208. [PubMed: 10724176]
31. Hu S, Smith KM, Spiro TG. Assignment of protoheme resonance Raman spectrum by heme labeling in myoglobin. J. Am. Chem. Soc. 1996; 118:12638–12646.
32. Andrew CR, George SJ, Lawson DM, Eady RR. Six- to five-coordinate heme-nitrosyl conversion in cytochrome *c′* and its relevance to guanylate cyclase. Biochemistry. 2002; 41:2353–2360. [PubMed: 11841228]
33. Lawson DM, Stevenson CE, Andrew CR, George SJ, Eady RR. A two-faced molecule offers NO explanation: the proximal binding of nitric oxide to haem. Biochem. Soc. Trans. 2003; 31:553–557. [PubMed: 12773155]
34. Zhao Y, Brandish PE, Ballou DP, Marletta MA. A molecular basis for nitric oxide sensing by soluble guanylate cyclase. Proc. Natl. Acad. Sci. U. S. A. 1999; 96:14753–14758. [PubMed: 10611285]
35. Martin E, Berka V, Sharina I, Tsai AL. Mechanism of binding of NO to soluble guanylyl cyclase: implication for the second NO binding to the heme proximal site. Biochemistry. 2012; 51:2737–2746. [PubMed: 22401134]

36. Lorković I, Ford PC. Nitric Oxide Addition to the Ferrous Nitrosyl Porphyrins Fe(P)(NO) Gives trans-Fe(P)(NO)2 in Low-Temperature Solutions. Journal of the American Chemical Society. 2000; 122:6516–6517.

37. Moënne-Loccoz P, de Vries S. Structural characterization of the catalytic high-spin heme *b* of nitric oxide reductase: A resonance Raman study. J. Am. Chem. Soc. 1998; 120:5147–5152.

38. Moënne-Loccoz P, Richter O-MH, Huang HW, Wasser IM, Ghiladi RA, Karlin KD, de Vries S. Nitric oxide reductase from *Paracoccus denitrificans* contains an oxo-bridged heme/non-heme diiron center. J. Am. Chem. Soc. 2000; 122:9344–9345.

39. Duarte AG, Cordas CM, Moura JJ, Moura I, Cordas CM, Duarte AG, Moura JJ, Moura I, Timoteo CG, Pereira AS, Martins CE, Naik SG, Duarte AG, Moura JJ, Tavares P, Huynh BH, Moura I. Steady-state kinetics with nitric oxide reductase (NOR): New considerations on substrate inhibition profile and catalytic mechanism. Biochim. Biophys. Acta. 2014; 1837:375–384. [PubMed: 24412239]

40. Girsch P, de Vries S. Purification and initial kinetic and spectroscopic characterization of NO reductase from *Paracoccus denitrificans*. Biochim. Biophys. Acta. 1997; 1318:202–216. [PubMed: 9030265]

41. Hendriks J, Warne A, Gohlke U, Haltia T, Ludovici C, Lubben M, Saraste M. The active site of the bacterial nitric oxide reductase is a dinuclear iron center. Biochemistry. 1998; 37:13102–13109. [PubMed: 9748316]

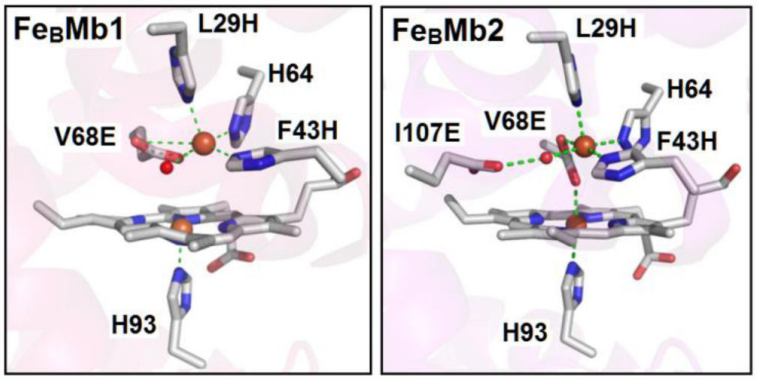

Figure 1.

Active site structures of Fe$_B$Mb1 (PDB entry 3K9Z) and Fe$_B$Mb2 (PDB entry 3M39).(14, 15)

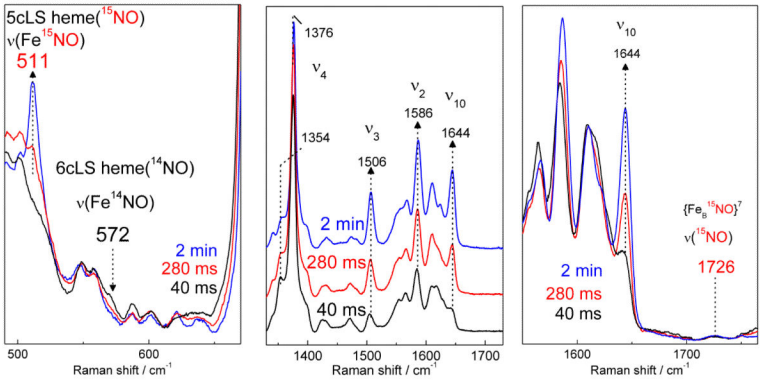

Figure 2.

RR spectra of RFQ samples of the reaction of $Fe_BMb1(^{14}NO)$ with a 3-fold ^{15}NO excess (excitation wavelength 406 nm, sample temperature 110 K).

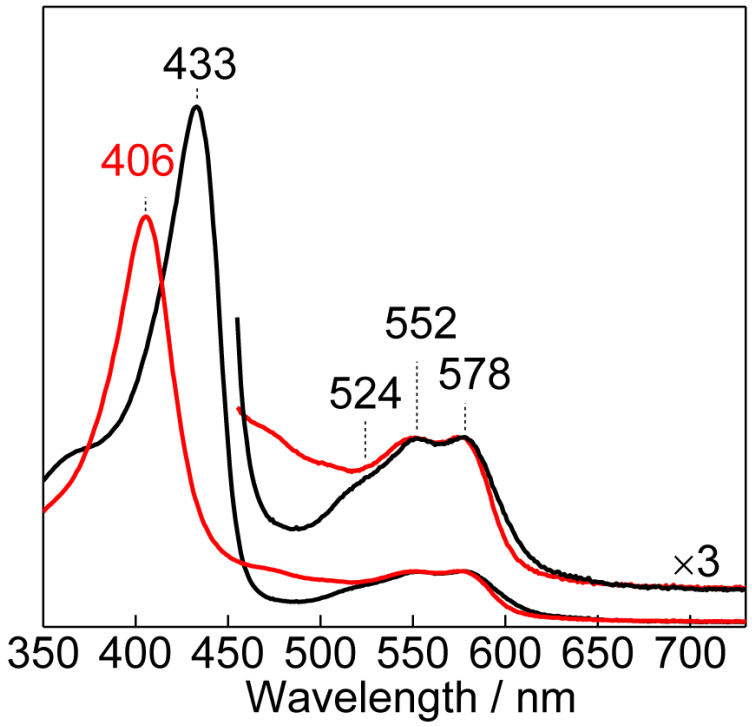

Figure 3.

Room temperature UV-vis absorption spectra of reduced Fe_BMb3 after loading of the Fe_B site with Fe(II) (black) and of the resting complex formed after exposure to 100 μM NO (red).

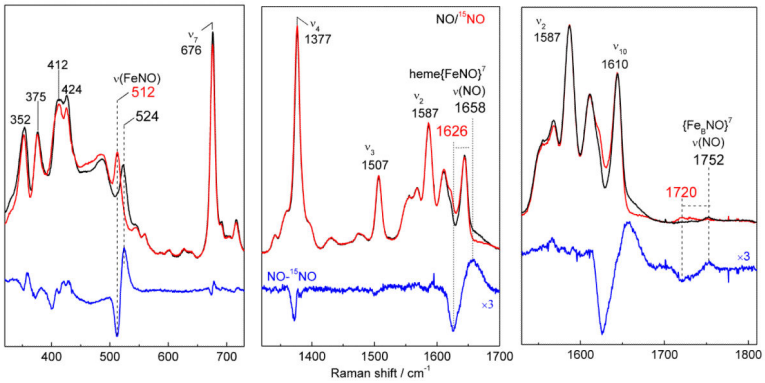

Figure 4.

RR spectra of the reaction end product of reduced Fe_BMb3 with 4-fold ^{14}NO excess (black traces) and ^{15}NO (red traces). Also shown are ^{14}NO – ^{15}NO differential signals for the nonheme ν(NO), heme ν(NO), and heme ν(FeNO) modes (blue traces) (excitation wavelength 406 nm, sample temperature 110 K).

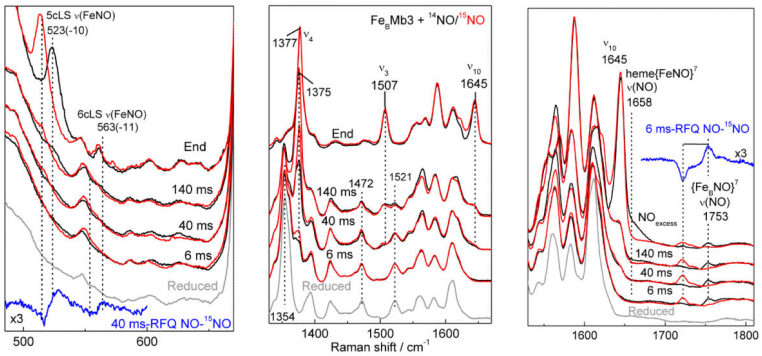

Figure 5.

RR spectra of RFQ samples of the reaction of reduced Fe_BMb3 with 3-fold ^{14}NO excess (black traces) or ^{15}NO (red traces) compared with those of resting reduced Fe_BMb3 (gray traces) (excitation wavelength 406 nm, sample temperature 110 K). Also shown are selected ^{14}NO – ^{15}NO differential signals for the nonheme ν(NO) and heme ν(FeNO) modes (blue traces).

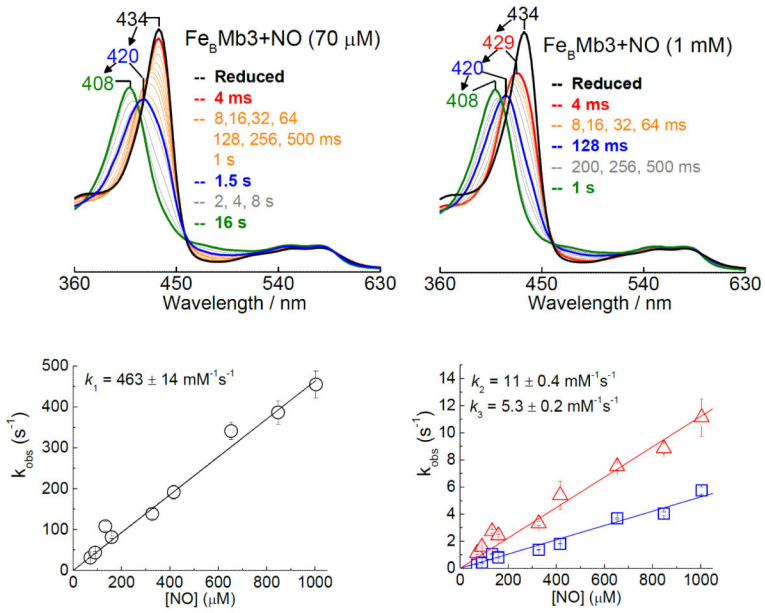

Figure 6.

Stopped-flow UV-vis absorption spectra of the reaction of reduced Fe$_B$Mb3 with 70 μM and 1 mM NO at 4 °C. Also shown are the dependence of observed rate constants on NO concentrations.

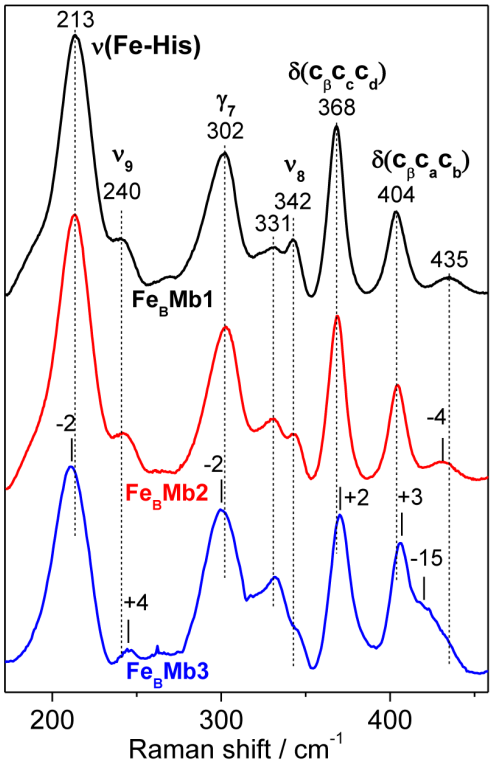

Figure 7.

Room-temperature RR spectra of the iron(II)-loaded reduced protein Fe_BMb1 (black), Fe_BMb2 (red), and Fe_BMb3 (blue) obtained with a 442-nm laser excitation.

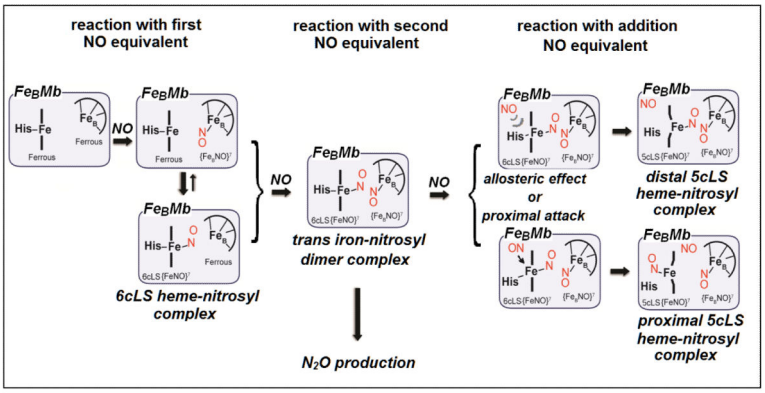

Scheme 1.
Reaction of reduced Fe_BMbs with NO.

Table 1

Rate constants for NO binding ($mM^{-1}s^{-1}$) at 4 °C and observed vibrational frequencies (cm^{-1}) of heme and nonheme $\{FeNO\}^7$ species in Fe_BMb constructs.

Proteins	NO association rates	6 to 5c nitrosyl conversion	5cLS heme $\{FeNO\}^7$		$\{FeBNO\}^7$	Reference
			ν(FeNO) (Δ^{15}N)	ν(NO) (Δ^{15}N)	ν(NO) (Δ^{15}N)	
Fe_BMb1	k_1 = 580, k_2 = 6.1	2.1	522 (−12)	1660 (−30)	1755 (−32)	JACS
Fe_BMb2	k_1 = 377, k_2 = 18	>1	-	-	1759 (−33)	JACS
Fe_BMb3	k_1 = 463, k_2 = 11	5.3	524 (−12)	1658 (−32)	1752 (−32)	This work